# Non-Newtonian Viscosity of Dilute Polymer Solutions

**R. Pamies, M. C. Lopez Martinez, J. G. Hernandez Cifre, and J. Garcia de la Torre***

*Departamento de Quimica Fisica, Facultad de Quimica, Universidad de Murcia, 30071 Murcia, Spain*

*Received August 24, 2004; Revised Manuscript Received October 15, 2004*

ABSTRACT: The non-Newtonian behavior of dilute polymer solutions is investigated by computer simulation of a bead-and-spring model, using the Brownian dynamics technique to evaluate the shear rate dependence of the intrinsic viscosity. This behavior is a consequence of the combined effects of hydrodynamic interaction, excluded volume, and finite extensibility. The simulations allow the study of the influence of each effect separately. When all the effects are considered, the simulation results can be compared to experimental data of solution viscosities, which are available just in the region of moderately small shear rates. Data from molecular architecture and other solution properties are obtained to parametrize the bead-and-spring model, with emphasis in the description of the chain extensibility. Comparison of simulation and experimental results is presented for both highly flexible vinyl polymers and locally stiff cellulose chains.

## 1. Introduction

The non-Newtonian behavior, i.e., the shear rate dependence of the viscosity, is one of the most characteristic properties of polymeric systems. It is well-known that even very dilute polymer solutions are non-Newtonian, which indicates that this phenomenon is inherent to the properties of individual polymer molecules. Several features of polymer chain statistics and dynamics can play some role in the non-Newtonian behavior: excluded volume, hydrodynamic interactions, chain extensibility, etc. Early attempts to investigate the effect of the different possible causes were made using classical polymer dynamics theory,[1−8] with somehow contradictory results.[9] Nowadays, computational methodologies like the Brownian dynamics (BD) or the molecular dynamics (MD) procedures allow an efficient simulation of the various effects (see, for instance, ref 10 for a review of computational models and methods). Indeed, there have been several recent descriptions of non-Newtonian behavior of dilute polymer solutions simulated in various model systems.[11−17] The numerical results are usually displayed as the dependence of intrinsic viscosity, $[\eta]$, on the flow strength, the latter being expressed either directly, as the shear rate, $\dot{\gamma}$, or in the form of a quantity involving polymer characteristics

$$\beta = \frac{[\eta]_0 \eta_0 M}{RT}\dot{\gamma} \tag{1}$$

where $M$ is the polymer molecular weight, $[\eta]_0$ the zero shear intrinsic viscosity of the solution, $\eta_0$ the viscosity of the solvent, $R$ the ideal gas constant, and $T$ the absolute temperature.

Experiments indicate that polymer solutions show a shear-thinning behavior, with $[\eta]$ decreasing with shear rate. Theoretical and computational results predict, under certain conditions (vide infra), this decrease. In typical graphs, with logarithmic scale for $\dot{\gamma}$ or $\beta$, there is a Newtonian plateau, with $[\eta] = [\eta]_0$, followed quite suddenly by a decay in $[\eta]$ of several orders of magnitude which obeys a power law, $[\eta] \propto \dot{\gamma}^{-\nu}$. Unfortunately, experimental results of the non-Newtonian behavior of very dilute polymer solutions are not systematic and abundant, and to the best of our knowledge, all the available results cover a range over which $[\eta]/[\eta]_0$ goes down to about 0.5, at most[18,19] (examples will be mentioned later), and clearly do not belong to the power-law region. It has been demonstrated that the strong, power-law decay at very high shear rates is essentially caused by the finite extensibility (FE) of the polymer chain,[12,20,21] although under certain circumstances EV effects could also lead to significant shear thinning at high shear.[22,23] However, in the range of moderate shear rates for which the decrease in $[\eta]$ is, say 10%−50%, the shear rate dependence may be rather influenced by the other effects: hydrodynamic interaction (HI) and excluded volume (EV).

In this paper we employ the Brownian dynamics (BD) simulation method to study the shear rate dependence of the intrinsic viscosity, with particular emphasis on the region of moderate shear rate where experimental data are available. We mention that at these shear rates chain scission is not expected. This phenomenon, out of the goal of the present paper, could appear at extremely high shear and can be studied following a similar procedure to that used to simulate the more common fracture in extensional flows.[24] We study the influence of the three effects: HI, EV, and FE, both separately and in combinations. In this way we can discuss the contribution of each effect, thus providing a better understanding of the non-Newtonian behavior of dilute polymer solution. Very recently, other authors[25] have also studied the influence of HI, EV, and FE on dilute polymer solutions with a more general purpose. To compare simulation results with experimental data, we describe how to assign values to the model parameters from information about molecular architecture of the polymer chain or from other solution properties. Predictions of BD simulations are compared to experimental data for polymers with different degree of chain extensibility.

* Corresponding author: phone +34 34968367426; Fax +34 34968364148; e-mail jgt@um.es.

10.1021/ma0482617 CCC: $30.25 
Published on Web 01/20/2005

## 2. Theory and Methods

The model that we adopt to describe the polymer molecule is a bead-and-spring chain in a continuous solvent of viscosity $\eta_0$. We employ FENE (finitely extensible, nonlinear elastic) springs with force constant $H = 3k_bT/b^2$ and maximum elongation $Q_{max}$, whose force law is given by the classical Warner equation.[26] Parameter $b$ in force constant expression is an arbitrary unit of length, which coincides with the mean-square spring length in the absence of flow, $\langle Q^2\rangle_0 = b^2$, when $Q_{max} \rightarrow \infty$ (i.e., for a Gaussian chain). The beads are spherical frictional elements with Stokes radius $\sigma = 0.25b$ and frictional coefficient $\zeta = 6\pi\eta_0\sigma$, which corresponds to the usually adopted value of the hydrodynamic interaction (HI) parameter $h^* = 0.25$. As it will be shown later (Figure 6), the exact value of $h^*$ is practically irrelevant for the results presented in this paper. In this work the number of beads is in the range $N = 15-40$, which we consider long enough to be representative of a long polymer chain but still feasible for the simulation work. (Indeed, as shown below, the model parametrization requires relatively low values for $N$.)

Good solvent conditions can be introduced by means of a Lennard-Jones excluded-volume (EV) potential with parameters $\sigma_{LJ} = 0.8b$ and $\epsilon_{LJ} = 0.1k_BT$.[27] Attempts have been made to relate Lennard-Jones parameters to the solvent quality.[28] Nevertheless, the limit of "perfect" good solvent conditions adopted in this work (e.g., $\sigma_{LJ} = 0.8b$ and $\epsilon_{LJ} = 0.1k_BT$) gives more than acceptable results provided $N$ is large enough. Monte Carlo simulations with several $N$ and good solvent conditions were performed in order to test the validity of the $N$ values employed. In the log−log plot of the radius of gyration vs $N$ (not shown here) we obtained all points aligned even for values of $N$ as low as 10, as well as the correct slope of about 0.6. Alternatively, EV effects can be ignored, which would correspond to an ideal chain. Hydrodynamic interactions (HI) are described by a Rotne−Prager−Yamakawa tensor.[29,30] For non very large chain lengths, as those used in this work, this implementation of HI presents a similar efficiency to that more sophisticated procedure based on the Chebyshev polynomial.[31] Although this effect is essential for a proper description of polymer dynamics in solution, sometimes it is interesting to neglect HI effect for comparative purposes. The polymer solution is subject to a simple, steady shear flow, whose velocity at the position of the $i$th bead with coordinates $(x_i, y_i, z_i)$ is $v_x = \dot{\gamma}y_i$, where $\dot{\gamma}$ is the shear rate.

In the computational work, quantities are handled in dimensionless forms, hereafter denoted with an asterisk. For lengths and dimension the unit is $u_l = b$, the unit of force is $u_F = k_BT/b$, and the unit of time is a characteristic time of the model chain given by $u_t = \zeta b^2/k_BT$, so that the reduced shear rate is $\dot{\gamma} = \dot{\gamma}u_t$. The intrinsic viscosity $[\eta]$ is conveniently expressed in a reduced form as $[\eta]^* = [\eta]M/(N_Au_l^3)$. This definition is irrelevant, as we shall present our main results as ratios $[\eta]/[\eta]_0$ where $[\eta]_0$ is the zero shear rate intrinsic viscosity, and this ratio is obviously identical to $[\eta]^*/[\eta]_0^*$.

Brownian dynamics (BD) simulation is used to simulate the evolution of the chain in the shear flow. We employ the predictor−corrector modification of Iniesta and García de la Torre[32] of the first-order Ermak−McCammon algorithm,[33] including the flow term.[34] The duration of the trajectory, typically $T^* = 2000$, is many times longer than the longest relaxation time of the chain. The time step is $\Delta t^* = 10^{-4}$ when Lennard-Jones EV is included, and $\Delta t^* = 10^{-3}$ when it is neglected. A number of conformations, typically $10^4$, are sampled uniformly along the Brownian trajectory. At each conformation, the cross-component of the stress tensor is evaluated as

$$\tau_{xy}^* = \sum_{i=1}^{N-1} (F_x^*)_i (Q_y^*)_i \tag{2}$$

where $(F_x)_i$ is the flow direction component of the force exerted by the $i$th spring and $(Q_y)_i$ is the gradient direction component of the $i$th connector vector. Because of stress tensor symmetry $\tau_{xy} = \tau_{yx}$. From the average of $\tau_{xy}$ over the sampled conformations, the intrinsic viscosity is evaluated as

$$[\eta]^* = -6\pi\sigma^*(\tau_{xy}^*/\dot{\gamma}^*) \tag{3}$$

It is pertinent to mention here that the calculation of shear viscosity from BD simulation is appreciably affected by numerical errors, particularly at the moderate or small shear rates that are significant for the analysis of experimental data. In shear, the viscosity is evaluated (eq 3) as the quotient of two small numbers; the cross-component of the stress tensor, $\tau_{xy}$, is small, and therefore the simulation uncertainties produce an appreciable relative error. Thus, the results at low $\dot{\gamma}$ will have a large error bar. The remedy is to run long simulations, but this is in conflict with the important increase in computing time with $N$ when hydrodynamic interaction is included, as required to predict realistic data. Because of the simulation errors at low $\dot{\gamma}$, the calculation of the zero shear rate intrinsic viscosity, $[\eta]_0^*$, by extrapolation of $[\eta]^*$ to $\dot{\gamma} = 0$ produces quite erroneous results. Then, we have adopted and alternative way, in which the zero shear intrinsic viscosity is evaluated by the so-called rigid-body treatment (RB).[35−37] As shown by Fixman,[38] the RB treatment is a lower bound that provides an approximation to the viscosity expected to deviate from the exact results by just a few percent (much less than the viscosity decrease due to shear thinning). Recently, other methods to obtain the zero shear rate intrinsic viscosity have been developed, most notably variance reduced simulations[39] and the use of Green−Kubo expressions.[40] We chose the RB treatment because of its less computational cost.

In previous works, the generation of conformations for the RB treatment was done using a Monte Carlo procedure. Currently, we employ for such purpose a no-flow BD simulation, which samples correctly the conformational space. Thus, no-HI, no-flow BD works as a "smart Monte Carlo" method.[41] Conformations are picked at regular intervals along the BD trajectory. The sample of conformations so generated is divided into five subsamples. From the conformational averages for each subsample, the final average is obtained, and the standard deviation of the five subsample average serves as an error bar.

Finally, in terms of $[\eta]_0^*$ and $\dot{\gamma}^*$, the quantity $\beta$ in eq 1, which is already dimensionless, can be derived from reduced quantities as

$$\beta = \frac{[\eta]_0^*\dot{\gamma}^*}{6\pi\sigma^*} \tag{4}$$

**Table 1. Reduced Zero Shear Intrinsic Viscosities Obtained from RB Calculations ($N = 37$, $Q^*_{max} = 5$)'**

| HI | EV | FE | $[\eta]^*_0$ |
|---|---|---|---|
| − | − | − | 182 ± 5 |
| + | − | − | 89 ± 2 |
| − | + | − | 320 ± 5 |
| + | + | − | 163 ± 2 |
| − | − | + | 164 ± 3 |
| + | − | + | 80.0 ± 1.1 |
| − | + | + | 316 ± 5 |
| + | + | + | 159 ± 2 |

## 3. Numerical Results

As stated in the Introduction, the first purpose of this paper is to describe the effect of the three molecular features: finite extensibility (FE), hydrodynamic interaction (HI), and excluded volume (EV) in the shear rate dependence of the intrinsic viscosity. Several cases can be considered in which one, two, or all of these effects are either included or ignored. The possible cases will be indicated with the notation ±HI±EV±FE, where + and − indicate inclusion or neglection, respectively. For this comparative study, which has an essentially theoretical purpose, we simulate a chain with $N = 37$ beads in all the possible combinations. For the reduced maximum spring extension we take $Q^*_{max} = 5$, which is in the middle of the range of values expected for typical experimental systems.

**3.1. Zero Shear Intrinsic Viscosity and Newtonian Case.** Values of the zero shear intrinsic viscosity in reduced form, $[\eta]^*_0$, needed for the ratios $[\eta]^*/[\eta]^*_0$ and for $\beta$, obtained by the RB procedure, are given in Table 1. It is evident that HI and EV have an important influence, while FE is unimportant in the limit of zero shear (except may be when it is the only effect considered, as also found by other authors[25]). The case −HI−EV−FE, which corresponds to a chain of Gaussian bonds without HI (a Rouse chain), can be compared with the exact result[20]

$$[\eta]^*_0 = \frac{\pi\sigma^*}{4}\sum_{j=1}^{N-1}\left[\sin\left(\frac{j\pi}{2N}\right)\right]^{-2} \tag{5}$$

or for $N$ large

$$[\eta]^*_0 = \frac{N^2\sigma^*}{\pi}\sum_{j=1}^{N-1} j^{-2} \tag{6}$$

Our RB result for the −HI−EV−FE case, $[\eta]^*_0 = 182 \pm 5$, agrees very well with results from eq 5 and eq 6, 179 and 176, respectively.

It is important to note that the effects of HI and EV on $[\eta]^*_0$ go in opposite directions: HI decreases the viscosity due to the hydrodynamic shielding, while EV increases chain size and therefore the viscosity, too. The same trends are expected in flows so that, as we will show immediately, the balance of these two effects is important in the non-Newtonian behavior.

It is well-known that the bead-and-spring chain with infinitely extensible springs, without excluded volume (Gaussian chain in the absence of flow) and without hydrodynamic interaction (Rouse model), predicts a Newtonian behavior over the whole range of shear rate. We have obtained results (not shown) for the −HI−EV−FE case, combining the $[\eta]^*$ from BD simulation with the $[\eta]^*_0$ from RB calculation. The results reproduce the

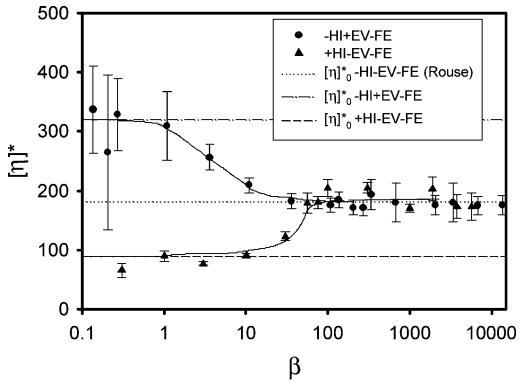


**Figure 1.** Reduced intrinsic viscosity, $[\eta]^*$, vs relative flow rate, $\beta$, for chains including either hydrodynamic interaction (+HI−EV−FE) or excluded volume (−HI+EV−FE). The horizontal lines mark the values of the zero shear intrinsic viscosity, $[\eta]^*_0$, in the −HI−EV−FE, +HI−EV−FE, and −HI+EV−FE cases.

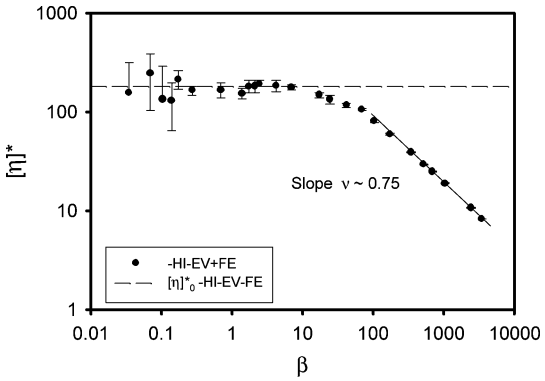


**Figure 2.** Reduced intrinsic viscosity, $[\eta]^*$, vs relative flow rate, $\beta$, for chains including only finite extensibility (−HI−EV+FE case).

independence of viscosity on shear rate: the ratio $[\eta]/[\eta]_0$, which must be unity in the Newtonian regime, has a mean value of 1.03 over the range $\beta = 10^{-1}$−$10^3$ of shear rate.

**3.2. Influence of HI, EV, and FE Separately.** Figure 1 displays the BD simulation results for chains including either hydrodynamic interaction or excluded volume. At low shear rates, the BD results are in agreement (within their noticeable error bar) with the corresponding $[\eta]^*_0$ from the RB calculation. As the shear rate is increased, the $[\eta]^*$ values change, and at very high shear rates, both cases reach asymptotically the zero shear rate value of the Rouse chain. This is in agreement with expectations from a simple, physical argument: at high shear the chain is very extended and (i) the excluded-volume effect disappears, and (ii) as the chain elements are far apart, the distance-dependent hydrodynamic interactions disappear also. Thus, in that limit both cases reduces to the Newtonian Rouse chain.

The inclusion of either the HI or the EV effects produces a shear rate dependence that goes from a Newtonian plateau at low shear rates, to reach another Newtonian plateau at high shear rates. The difference is that HI produces an increase in the viscosity with shear rate, while EV results in a decrease.

Now, the introduction of finitely extensibility in the absence of the two other effects give rise to a typical non-Newtonian behavior, illustrated in Figure 2, with a Newtonian plateau at low shear rates, followed immediately by an intense shear thinning, in which $[\eta]$

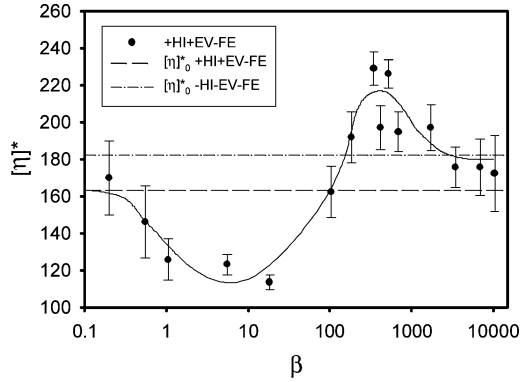


**Figure 3.** Reduced intrinsic viscosity, $[\eta]^*$, vs relative flow rate, $\beta$, for chains neglecting finite extensibility but including both hydrodynamic interaction and excluded volume (+HI+EV−FE case). The lower and upper horizontal lines mark the values of the zero shear intrinsic viscosities $[\eta]_0^*$ in the +HI+EV−FE and −HI−EV−FE cases.

follows a power law dependence, $[\eta] \propto \dot{\gamma}^{-\nu}$, or $[\eta] \propto \beta^{-\nu}$ with $\nu \approx 0.75$. This is the typical behavior arising from FE, remarkably different (qualitative and quantitatively) from that from HI and EV. The non-Newtonian viscosity due to FE is $[\eta] \ll [\eta]_0$ or $[\eta]/[\eta]_0 \ll 1$; however, as we will comment later on, the experimentally explored region is usually $[\eta]/[\eta]_0 \gtrsim 0.5$. Therefore, although FE is the effect that causes a most intense decrease in viscosity, we can anticipate that it will not be the only, or even the main contribution in the range covered by the experimental data.

**3.3. Combined Influence of Various Effects.** The combined effect of hydrodynamic interaction and excluded volume (+HI+EV−FE) case is shown in Figure 3. As commented for each individual effect, both must vanish at high shear rates, and therefore the shear rate dependence shows a transition from the value of $[\eta]_0^*$ (+HI+EV−FE) at zero or low shear rates to the value $[\eta]_0^*$ (−HI−EV−FE) at high shear rates. The BD simulation values in both limits seem to conform correctly this prediction.

Some years ago, the combined effect of HI and EV was studied either theoretically or by simulation using a dumbbell model ($N = 2$), with the result that there would be a monotonic decrease in the flow rate dependence, which would justify the experimentally observed thinning behavior.[11,42−44]

However, when the simplistic description based on the dumbbell is improved, using chains with an appreciably large number of elements ($N = 37$ in this study), it is clear that the result for the dumbbell is an artifact caused by the extremely simplicity of this model. The non-Newtonian behavior +EV+HI shows the compensation of the opposite influence of the two effects, which were displayed separately in Figure 1: there is, first, a decrease due to the weakening of the EV effect, which is followed by an increase due to the weakening of the HI effect. From elementary polymer solution dynamics, $[\eta]_0$ (−HI−EV−FE), i.e., the high-shear rate limit, must be larger than the low-shear value, $[\eta]_0$ (+HI+EV−FE), for a sufficiently long chain (recall that the former scales with chain length as $N^1$, while the latter goes as $N^{0.8}$ in good solvents). So, the overall +HI+EV should be a shear thickening, contrary to the experimental behavior. This situation was already anticipated in previous studies that employed chains instead of dumbbells.[11,13,45] At intermediate shear, the compensation of the two

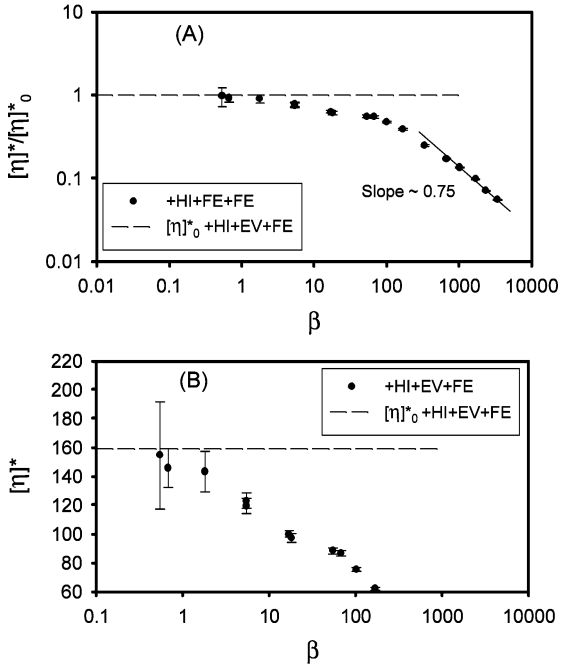


**Figure 4.** (A) Ratio $[\eta]/[\eta]_0$ vs relative flow rate, $\beta$, for the case +HI+EV+FE. (B) $[\eta]^*$ in a linear scale, and a limited range ($[\eta]/[\eta]_0 \approx 1...0.5$), again vs $\beta$.

effects may produce an oscillation in the shear rate dependence, which is clearly noticeable in Figure 3.

In the cases which either EV or HI is combined with FE, the appearance of the results is an obvious consequence of the previous observations. (For instance, a thorough discussion of the case +HI−EV+FE is found in ref 46.) At low shear rates, the first effect determines a moderate decrease or increase in the viscosity, but the high-shear plateau disappears and is replaced by the abrupt, monotonic decrease due to FE.

Finally, the most relevant and practically important case is that of combining all the effects; (+HI+EV+FE) values are displayed in Figure 4. The log−log plot that is sometimes employed to show the non-Newtonian behavior (Figure 4A) illustrates the power law regime at very high shear rates (say, beyond $\beta \approx 200$), where the viscosity decreases by one or more powers of ten. This feature replaces the high-shear plateau obtained in the −FE cases. However, at intermediate shear (say, in the range $\beta \approx 10-200$), there is an interesting feature that looks like a plateau or shoulder in the curve described by the data points. Depending on the model parameters ($N$ and $Q^*_{max}$) there could be even an ondulation; interestingly, this has been predicted by other authors.[47,48] In this region, $[\eta]$ decays to about half of the zero shear value. Another perspective is provided if the ordinate is not the ratio but the viscosity itself (Figure 4B); it is then apparent that $[\eta]$ decreases with shear rate beyond $\beta \approx 1$, reaching values about half of the zero shear rate value. HI and EV play also an important role (modulated by FE) in this region, which is the relevant one in the analysis of experimental results, as discussed in the next section.

## 4. Comparison with Experimental Data

**4.1. Model Parametrization.** As shown in the previous section, the BD simulation provides results for the intrinsic viscosity ratios, $[\eta]/[\eta]_0$, vs the reduced shear rate, $\beta$. These results can be directly compared

with experimental data, which are usually presented in terms of these two quantities. The comparison requires the assignation of values to the two model parameters, $N$ and $Q^*_{max}$. For this purpose, we introduce a quantity, $E$, which gauges the extensibility of the polymer chain, defined as the ratio of the fully extended length, $L$, to the mean-square radius of gyration of the coil at rest, $R_g \equiv \langle s^2 \rangle_0^{1/2}$.[49] This quantity can be evaluated both for the experimental system and for the simulated model as well, since $L^* = (N - 1)Q^*_{max}$ and $\langle s^{*2} \rangle_0$ can be evaluated by simulation:

$$E = \frac{L}{R_g} = \frac{(N-1)Q^*_{max}}{\langle s^{*2} \rangle_0^{1/2}} \tag{7}$$

Provided with the experimental value of $E$, the model is parametrized as follows. The number of elements, $N$, is given an arbitrary value, sufficiently large but still moderate so that the computing time required to generate the BD trajectory is within our reach. Previous BD no-HI simulations without flow have been made to determine the dependency of $\langle s^{*2} \rangle_0$ and therefore $E$ on $Q^*_{max}$ and $N$. Then, for the value assigned to $N$ and the experimental $E$, the corresponding $Q^*_{max}$ is found by interpolation. Trials with various $N$'s reveal that the computed results are practically independent of this choice. Then, as $Q^*_{max}$ is determined from separate experiments, it can be somehow affirmed that our simulation of $[\eta]/[\eta]_0$ vs $\beta$ does not involve adjustable parameters.

Examples of the parametrization and results of non-Newtonian viscosities are next presented for various cases. We have actually considered two kinds of systems composed of polymers with typically flexible or stiff local structures, which therefore differ appreciably in their extensibility.

**4.2. Locally Flexible Chains: Vinyl Polymers.** The chain skeleton of vinyl polymers is rather flexible: a few tens of repeating units, with molecular weight of $10^3-10^4$ g/mol, is sufficient for the chain to present the typical Gaussian coil statistics.[50] Their fully extended length can be estimated from that of the chain in the all-trans conformation, given by

$$L = (2M/M_1)d_{C-C} \cos[(\pi - \theta)/2] \tag{8}$$

where $M_1$ is the molecular weight of the repeating unit, so that $2M/M_1$ is the number of C−C bonds, that have a bond length $d_{C-C} = 1.54 \times 10^{-8}$ cm and a bond angle $\theta = 110°$. The radius of gyration is usually available from light scattering measurements, or alternatively it can be estimated from other solution properties, such as the intrinsic viscosity or the diffusion coefficient. Thus, the extensibility of vinyl polymers can be readily determined.

Figure 5A displays the shear rate intrinsic viscosity of poly(α-methylstyrene) of $M = 7.52 \times 10^6$ g/mol in toluene at 25 °C (good solvent conditions). At zero shear rate, $[\eta]_0 = 950$ cm $^3$/g. Experimental data are from Noda et al.[18] The radius of gyration is computed using the Flory−Fox relationship for good solvent conditions (i.e., with the Flory parameter $\Phi = 1.9 \times 10^{23}$). Thus, $R_g = [M[\eta]_0/(6^{3/2}\Phi)]^{1/3} = 13.68 \times 10^{-6}$ cm. With $M_1 = 118$ g/mol, we obtain $L = 16.07 \times 10^{-4}$ cm, which yields $E = 117.5$ for this system. For the simulation, we have tried two choices for the number of beads, $N = 17$ and 37, for which the value of $E$ corresponds to $Q^*_{max} = 14.9$ and 10.7, respectively. The results show that, within the simulation uncertainties, the two choices are practically equivalent, and the agreement with the experimental data is good. Some simulation results without HI and without EV are also shown to demonstrate the importance of these effects in predicting the viscosity behavior at low shear rate. FENE springs at low shear tend to be Gaussian, and viscosity remains constant in the absence of other effects. Figure 5B shows similar results for polystyrene in benzene at 20 °C, with $[\eta]_0 = 830$ cm$^3$/g[52] and $M = 5.1 \times 10^6$ g/mol (computed from the viscometric equation $[\eta]_0 = 12.3 \times 10^{-3} M^{0.7251}$). With an analogous calculation to that perform with the former vinyl polymer, we get for this polystyrene $L = 12.37 \times 10^{-4}$ cm (with $M_1 = 104$ g/mol) and $R_g = 11.49 \times 10^{-6}$ cm, which yields $E = 107.6$. The comparison with simulation data confirms the conclusions from the previous system.

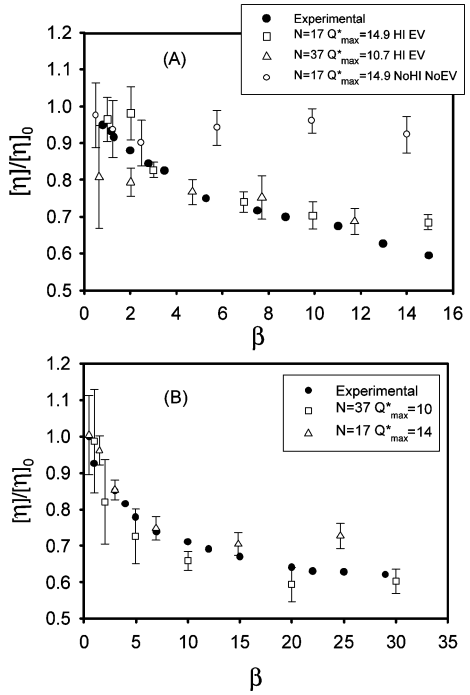


**Figure 5.** Experimental and simulation results for (A) poly(α-methylstyrene) in toluene and (B) polystyrene in benzene. See text for further details.

**4.3. Locally Stiff Chains: Cellulose Derivatives.** Polymers (usually of biological origin, like DNA and polysaccharides) with a locally stiff structure show a pronounced shear rate dependence of the solution viscosity and therefore have been employed for experimental studies of the non-Newtonian behavior. This polymers, when they are long enough, are in the random coil limit of the wormlike chain model, and the present methodology is applicable. However, the number of Kuhn segments is small, and their extensibility is appreciably smaller than that for more flexible polymers. For these macromolecules, the parameters of the wormlike model are used to characterize the chain; these are the persistence length, $P$, and the mass per unit length, $M_L = M/L$. For the evaluation of their extensibility, we have $L = M/M_L$, and $R_g$ (if not directly available) can be obtained from the expression for the coil limit of the wormlike model, $R_g^2 = PL/3$, so that $E = (3M/PM_L)^{1/2}$.

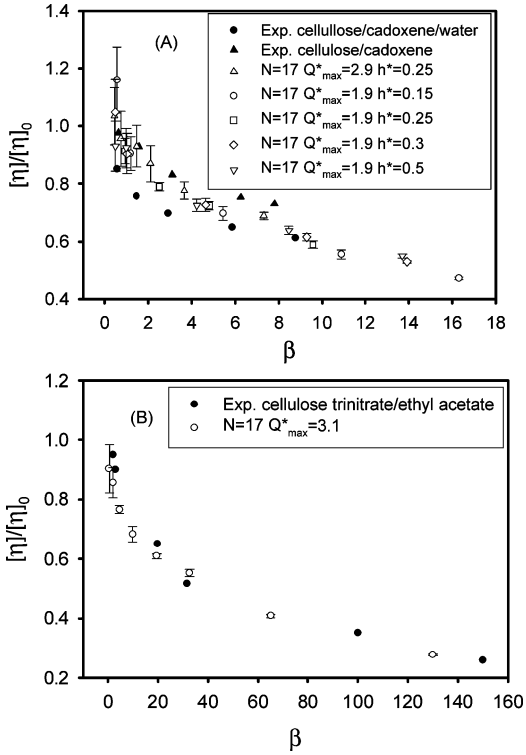


**Figure 6.** Experimental and simulation results for (A) cellulose in cadoxene/water (black circles) and cellulose in cadoxene (black triangles) and (B) cellulose trinitrate in ethyl acetate. See text for further details.

A systematic and careful experimental study of the non-Newtonian viscosity of cellulose polymers has been reported by Riande and Pereña.[19] In Figure 6A we show their results for cellulose in cadoxene/water (1:1) at 25 C with $M = 4.29 \times 10^5$ g/mol and $[\eta]_0 = 843$ cm$^3$/g as well as cellulose in cadoxene with $M = 3.3 \times 10^5$ g/mol and $[\eta]_0 = 643$ cm$^3$/g. Among the systems that they studied, the former is the one with a more pronounced decrease in viscosity. Unfortunately, the molecular weight per unit length of these systems is not found in the literature. In ref 19, authors state that the statistical chain element (Kuhn step) for cellulose can be considered to be about 10 nm, so that the persistence length can be set to $P \simeq 5$ nm. From data for cellulose trinitrate,[53] we estimate $M_L \approx 450$ nm$^{-1}$, which along with the value of $P$ above yields $E \simeq 23.9$ for the system cellulose in cadoxene/water. On the other hand, in ref 54 we find that the persistence length of cellulose in cadoxene is about 7 nm, which yields $E \simeq 17.7$ for the second system considered. Note that for these polymers $E$ is much smaller than for vinyl polymers. As a consequence, the values of $Q^*_{max}$ are rather small; thus, we have, considering $N = 17$, $Q^*_{max} = 2.9$ and 1.9 for cellulose in cadoxene/water and cellulose in cadoxene, respectively. The agreement between simulation and experiments in these cases is not fully satisfactory. Surprisingly, the case with smaller estimated extensibility, cellulose in cadoxene with $M = 3.3 \times 10^5$ g/mol, is better reproduced by the chain model with higher extensibility, $E \simeq 23.9$. The disagreements may be due (apart from the uncertainty in the data for $P$ and $M_L$) to the fact that these cases are at the limit of validity of our treatment. For very low $Q^*_{max}$ (close to the equilibrium elongation at rest) the Warner law for the FENE spring may be unrealistic. For a given $E$, higher $Q^*_{max}$ would correspond to even lower $N$, for which the model chain could be unrealistic again. A point to consider is that in the FENE model the value chosen for the hydrodynamic parameter, $h^*$, could have some influence on results,[55] mainly at small $Q^*_{max}$. In Figure 6A we include results carried out for a reasonable $h^*$ range;[55] these results demonstrate that the values of $[\eta]/[\eta]_0$ are practically independent of the exact value of $h^*$ for the range of $\beta$ used, even in the most unfavorable simulation conditions, e.g., $N = 17$ and $Q^*_{max} = 1.9$. In the related system cellulose trinitrate in ethyl acetate at 25 °C (now a theta system),[56] discussed also in ref 19, the agreement is much better as it is observed in Figure 6B. Experimental points shown in that figure are taken from Figure 12 in ref 19. Riande and Pereña find a good fit of those experimental data with the theoretical curve for $\lambda L = L/2P = 100$, which gives us directly an estimate for the extensibility: $E = (3L/P)^{1/2} = 24.5$. This value of $E$ corresponds to the simulation parameters $N = 17$ and $Q^*_{max} = 3.1$, which are in the range of validity of our FENE model.

## 5. Concluding Remarks

The early theories of non-Newtonian viscosity usually focused on one or some of the aspects that determine the shear rate dependence, and in most instances the main result was an equation for low shear rates, of the form

$$[\eta]/[\eta]_0 = 1 - Q\beta^n \tag{9}$$

where $Q$ is a constant that is not relevant for the present discussion. Various theories coincided finding $n = 2$.[3−5] According to this prediction, the curvature in the variation of $[\eta]/[\eta]_0$ with $\beta$ should be convex, with an initial zero slope. Some experimental studies find, at extremely low shear rate, a very slight variation of $[\eta]/[\eta]_0$ with $\beta$ which suggests an initial zero slope compatible with $n = 2$ (see for instance ref 57). However, other experimental values (Figures 5 and 6 and other cases that we have examined) and the simulation results do not support this prediction. Instead, data show an initially strong decrease of $[\eta]/[\eta]_0$ with $\beta$, which is less pronounced at higher $\beta$. This situation was noticed by several experimental workers (for instance, Lohmander and Svensson[56] and Golub[58] suggest $n = 1$). One of the early theories due to Bueche[2] reached a different result, with $n = 1/2$, which predicts concave curvature and strong initial decrease, in better agreement with many observations and our simulations.

Adequate understanding and numerical predictions for the non-Newtonian viscosity of dilute solutions can be achieved nowadays using Brownian dynamics simulation, as illustrated in this and other works. We have emphasized that BD calculations must be aimed to simulate the experimental results, which concentrate on the region of low shear rate where, unfortunately, the simulation results are rather sensitive to numerical uncertainties. That is, perhaps, the reason why other BD simulations have mainly displayed the region of very high shear rate, thus avoiding comparison with experiments. Our detailed description of the influence of the various features in the model (not only FE but also HI and EV) shows that all of them contribute, in a mixed manner, in that region. At the cost of a considerable computing time, BD provides sufficiently accurate predictions, that agree well with experimental results.

**Acknowledgment.** This work was supported by Grant BQU2003-04517 from Ministerio de Ciencia y Tecnologıa. R.P. acknowledges a FPU predoctoral fellowship, and J.G.H.C. is the recipient of a Ramón y Cajal postdoctoral research contract.

## References and Notes

(1) Kuhn, W.; Kuhn, H. *Helv. Chim. Acta* **1945**, *28*, 1533.
(2) Bueche, F. *J. Chem. Phys.* **1954**, *22*, 603−609.
(3) Peterlin, A.; Copic, M. *J. Appl. Phys.* **1956**, *27*, 434.
(4) Ikeda, Y. *J. Phys. Soc. Jpn.* **1957**, *12*, 378.
(5) Cerf, R. *J. Phys. Radium* **1958**, *19*, 122.
(6) Peterlin, A. *J. Chem. Phys.* **1960**, *33*, 1799.
(7) Subirana, J. A. *J. Chem. Phys.* **1964**, *41*, 3852−3856.
(8) Fixman, M. *J. Chem. Phys.* **1966**, *45*, 793−803.
(9) Yang, J. T. *Adv. Protein Chem* **1961**, *16*, 323−400.
(10) Kröger, M. *Phys. Rep.* **2004**, *390*, 453−551.
(11) López Cascales, J. J.; García de la Torre, J. *Polymer* **1991**, *32*, 3359−3363.
(12) van den Brule, B. H. A. A. *J. Non-Newtonian Fluid Mech.* **1993**, *47*, 357−378.
(13) Knudsen, K. D.; Elgsaeter, A.; García de la Torre, J. *Polymer* **1996**, *37*, 1317−1322.
(14) Lyulin, A. V.; Adolf, D. B.; Davis, G. R. *J. Chem. Phys.* **1999**, *111*, 758−771.
(15) Petera, D.; Muthukumar, M. *J. Chem. Phys.* **1999**, *111*, 7614−7623.
(16) Aust, C.; Kröger, M.; Hess, S. *Macromolecules* **1999**, *32*, 5660−5672.
(17) Prakash, J. R. *J. Rheol.* **2002**, *46*, 1353−1380.
(18) Noda, I.; Yamada, Y.; Nagasawa, M. *J. Phys. Chem.* **1968**, *72*, 2890−2898.
(19) Riande, E.; Pereña, J. M. *Makromol. Chem.* **1974**, *175*, 2923−2938.
(20) Bird, R. B.; Curtiss, C. F.; Armstrong, R. C.; Hassager, O. *Dynamics of Polymeric Liquids, Kinetic Theory*, 2nd ed.; John Wiley and Sons: New York, 1987; Vol. 2.
(21) Wedgewood, L. E.; Öttinger, H. C. *J. Non-Newtonian Fluid Mech.* **1988**, *27*, 245−264.
(22) Öttinger, H. C. *Phys. Rev. A* **1989**, *40*, 2664−2671.
(23) Kumar, K. S.; Prakash, J. R. *J. Chem. Phys.* **2004**, *121*, 3886−3897.
(24) López Cascales, J. J.; García de la Torre, J. *J. Chem. Phys.* **1991**, *95*, 9384−9392.
(25) Prabhakar, R.; Prakash, J. R. *J. Non-Newtonian Fluid Mech.* **2004**, *116*, 163−182.
(26) Warner, H. R. *Ind. Eng. Chem. Fundam.* **1972**, *11*, 379−387.
(27) Rey, A.; Freire, J. J.; García de la Torre, J. *Macromolecules* **1987**, *20*, 342−346.
(28) Graessley, W. W.; Hayward, R. C.; Grest, G. S. *Macromolecules* **1999**, *32*, 3510−3517.
(29) Rotne, J.; Prager, S. *J. Chem. Phys.* **1969**, *50*, 4831−4837.
(30) Yamakawa, H. *J. Chem. Phys.* **1970**, *53*, 436−443.
(31) Fixman, M. *Macromolecules* **1986**, *19*, 1204−1207.
(32) Iniesta, A.; García de la Torre, J. *J. Chem. Phys.* **1990**, *92*, 2015−2019.
(33) Ermak, D. L.; McCammon, J. A. *J. Chem. Phys.* **1978**, *69*, 1352−1360.
(34) Hernández Cifre, J. G.; García de la Torre, J. *J. Rheol.* **1999**, *43*, 339−358.
(35) Zimm, B. H. *Macromolecules* **1980**, *13*, 592−602.
(36) García de la Torre, J.; Jiménez, A.; Freire, J. J. *Macromolecules* **1982**, *15*, 148−154.
(37) García de la Torre, J.; López Martınez, M. C.; Tirado, M. M.; Freire, J. J. *Macromolecules* **1984**, *17*, 2715−2722.
(38) Fixman, M. *J. Chem. Phys.* **1982**, *76*, 6124−6132.
(39) Melchior, M.; Ottinger, H. C. *J. Chem. Phys.* **1996**, *105*, 3316−3331.
(40) Prabhakar, R.; Prakash, J. R. *J. Rheol.* **2002**, *46*, 1191−1220.
(41) Rossky, P. J.; Doll, J. D.; Friedman, H. L. *J. Chem. Phys.* **1978**, *69*, 4628−4634.
(42) López de Haro, M.; Rubı, J. M. *J. Chem. Phys.* **1988**, *88*, 1248−1252.
(43) Dıaz-Guilera, A.; Rubı, J. M.; Bedeaux, D. *Physica A* **1989**, *154*, 257−270.
(44) Zylka, W.; Öttinger, H. C. *J. Chem. Phys.* **1989**, *90*, 474−480.
(45) Zylka, W. *J. Chem. Phys.* **1991**, *94*, 4628−4636.
(46) Kishbaugh, A. J.; McHugh, A. J. *J. Non-Newtonian Fluid Mech.* **1990**, *34*, 181−206.
(47) Ganazzoli, F.; Tacconelli, A. *Macromol. Theor. Simul.* **1998**, *7*, 79−90.
(48) Ganazzoli, F.; Raffaini, G. *Macromol. Theor. Simul.* **1999**, *8*, 234−246.
(49) Hernández Cifre, J. G. Conformación y dinámica de macromoléculas flexibles en disoluciones sometidas a flujos. Ph.D. Thesis, Murcia, 2000.
(50) Flory, P. J. *Statistical Mechanics of Chain Molecules*, 1st ed.; John Wiley: New York, 1969.
(51) Kurata, M.; Tsunashima, Y. *Viscosity-Molecular Weight Relationships and Unperturbed Dimensions of Linear Chain Molecules*, 3rd ed.; Wiley: New York, 1988.
(52) Copic, M. *J. Phys. Chim.* **1957**, *54*, 348−355.
(53) Bohdanecky, M. *Macromolecules* **1983**, *16*, 1483−1492.
(54) Lapasin, R.; Pricl, S. *Rheology of Industrial Polysaccharides: Theory and Applications*, 1st ed.; Aspen: Gaithersburg, MD, 1999.
(55) Öttinger, H. C. *J. Non-Newtonian Fluid Mech.* **1987**, *26*, 207−246.
(56) Lohmander, U.; Svensson, A. *Makromol. Chem.* **1963**, *65*, 202−223.
(57) Zimm, B.; Crothers, D. M. *Proc. Natl. Acad. Sci. U.S.A.* **1962**, *48*, 905−911.
(58) Golub, M. A. *J. Phys. Chem.* **1956**, *60*, 431−435.

MA0482617